

# Magnetic properties and structure of electrodeposited Zn–Co alloys granular thin films

L. Vlad\*, P. Pascariu, S.I. Tanase, D. Pinzaru, M. Dobromir, V. Nica, V. Georgescu

Faculty of Physics, Alexandru Ioan Cuza University, Bd. Carol I, No. 11, Iasi 700506, Romania

## ARTICLE INFO

### Article history:

Received 14 November 2010

Received in revised form

21 January 2011

Accepted 22 January 2011

Available online 31 January 2011

### Keywords:

Electrodeposition

Zn–Co alloy

Zinc base alloys

Hysteresis – magnetic

X-ray photoelectron spectroscopy

## ABSTRACT

We present several results concerning the preparation by means of electrolysis and characterization of Zn–Co alloys thin films. Films of Zn, Co and Zn–Co with various compositions (8–16 at% Co) were prepared in sulfate baths, using potentiostatic control, envisaging applications in the domain of corrosion resistant magnetic sensors. The effects of applied voltage on the magnetic properties, microstructure and phase content of the electrodeposited Zn–Co films were investigated. The applied voltage significantly influenced the film composition and their magnetic properties. These films, when deposited at an applied voltage of 4.5 V exhibited multiphase behavior due to the inclusion of new phases (cobalt hydroxide), whereas at 3.0 V, only Zn–Co alloys were deposited. The structure and morphology of the samples were characterized by X-ray diffraction (XRD), X-ray photoelectron spectroscopy (XPS) and atomic force microscopy (AFM).

© 2011 Elsevier B.V. All rights reserved.

## 1. Introduction

The granular magnetic systems consisting of nanometer-sized ferromagnetic clusters have drawn a lot of attention in recent years due to the giant magnetoresistance (GMR) effect present in these materials [1,2]. With the purpose to make such kind of materials, we have chosen a system of alloys with limited solubility in solid state, displaying a tendency to form heterophase alloys, namely Zn–Co system. Zinc–cobalt alloys exhibit a significant corrosion resistance and we suppose that it could be possible for them to have an interesting magnetic behavior, unstudied yet. Taking into account the phase diagram of the system, we assume that it is possible to obtain granular alloys containing ferromagnetic/nonferromagnetic phases resulting in unusual magnetic and electric transport properties. We have chosen electrodeposition as a method of Zn–Co film preparation; this is a versatile technique for producing nanocrystalline deposits. Until now, the electrodeposition of Zn [3] and Zn–Ni or Zn–Co alloys has been studied especially because these alloys improve the corrosion resistance of a pure zinc coating [4–7]. It is necessary to understand the deposition mechanism in order to control the properties of the different deposits. As characterized by Brenner [8], the electrodeposition of Zn–Co alloys is considered a codeposition of anomalous type; that is, the less noble component (zinc) deposits preferentially compared to the more noble

one (cobalt). Because of this and because of the anticipated type of envisaged applications, the cobalt content in the Zn–Co alloy studied in published papers [8,9] is low (less than 10 at% Co); some studies have reported higher Co content in Zn–Co alloys obtained in alkaline electrolyte [10]. Fe–Ni, Co–Ni and Zn–Ni alloys are a few other examples of alloy systems, which have exhibited anomalous behavior in electrodeposition.

The aim of the present work is to obtain Zn–Co granular films by electrodeposition and to study the effects of the applied voltage on the structure, on the magnetic properties of the films, correlated with the deposition parameters; this study is of interest for potential applications in spintronics.

## 2. Experimental details

Electrodeposition was performed in potentiostatic regime using a cell with three electrodes, and by using platinum anode and a working electrode of copper Cu (1 0 0) textured foils; the reference electrode consisted of a platinum wire having the contact area with the electrochemical solution of 0.06 mm<sup>2</sup>. The working electrode of Cu and the platinum anode were vertically placed with disk-shaped foils, with only one side of the foil in contact with the electrolyte. The geometrical area of the working electrode was 3.14 cm<sup>2</sup>, same as the anode area.

By depositing some thick (500 nm) films of Zn, Co and Zn–Co alloys in fixed electrolytic conditions, we determined the electrodeposition rate. For these films the weights of the deposits were measured with a microbalance, having an estimated error of

\* Corresponding author. Tel.: +40 232201167; fax: +40 232201050.  
E-mail address: [laviniaivlad@gmail.com](mailto:laviniaivlad@gmail.com) (L. Vlad).

$\pm 10^{-6}$  g. In addition, a MII-4 Linnik interferential microscope was used to measure the thickness of these films using the multiple-beam Fizeau fringe method, in the reflection of monochromatic light.

Voltammetry obtained in the working cell was employed in the study of electrodeposition processes. From voltammetric results, the potentials or current densities were selected, which are more suitable to achieve alloy deposition.

In this paper we have approached the study of the structural properties and morphology of the samples using the following techniques: X-ray diffraction (SHIMADZU, XRD-6000) using  $\text{CuK}\alpha$  radiation (1.5406 Å) in the usual ( $\theta$ - $2\theta$ ) geometry, atomic force microscopy (AFM-NT-MDT Solver Pro-M) and X-ray photoelectron spectroscopy (XPS-PHI 5000 VersaProbe, ULVAC-PHI, INC). X-ray diffraction line broadening analysis has been used to estimate the average grain size by the Scherrer method [7,11,12].

Magnetic measurements were carried out at room temperature with a torsion magnetometer in the maximum field of 300 kA/m and using an induction type device with data acquisition system and ac magnetic field applied in the film plane (50 Hz, in 60 kA/m maximum field).

### 3. Results and discussion

We have started the research by experiments on electrodeposition performed separately of Zn and Co elements, in order to optimize the solution composition and deposition parameters. After that, the experiments were carried out for the Zn–Co alloy deposition from the sulfate baths of the composition given in Table 1. The deposition of Co films was performed from the solution labeled C, presented in Table 1, containing  $\text{CoSO}_4 \cdot 7\text{H}_2\text{O}$  as a base salt. For deposition of Zn films, the solution (labeled Z) contained mainly  $\text{ZnSO}_4 \cdot 7\text{H}_2\text{O}$  and  $\text{Zn}(\text{O}_2\text{CCH}_3)_2(\text{H}_2\text{O})_2$ . The solution (labeled ZC) for electrodeposition of Zn–Co alloys contains compounds of the two metals and a similar content of additives ( $\text{H}_3\text{BO}_3$ ,  $\text{Na}_2\text{SO}_4 \cdot 10\text{H}_2\text{O}$ , NaCl and triethanolamine). All solutions were freshly prepared with double distilled water. The temperature and pH values were kept at  $21 \pm 1$  °C and 5.0, respectively, without stirring the electrolyte. The film thickness for all the samples was controlled by electric charge passing through the electrolyte. The nominal thickness of the Zn, Co and Zn–Co alloy films was around 500 nm.

Voltammetric experiments were conducted in order to study the electrodeposition process of Zn–Co film. For that, cathodic polarization was carried out on Cu (1 0 0) substrate and completed by chronopotentiometric experiments conducted at the bias potential used to prepare the deposits. As an example for voltammetric studies, we present in Fig. 1 the variation of current density with cathode potential (versus Pt reference electrode) for the solutions Z, C and ZC (Table 1). From this figure one can see that the electrodeposition of a less noble element (Zn) shifts into more negative potentials for alloy electrodeposition compared to the electrodeposition of pure elements (i.e. Zn, Co). The electro-reduction of  $\text{Zn}^{2+}$  occurs at  $-0.92$  V from solution Z, and at  $-1.04$  V for the Zn–Co alloys electrodeposition (solution ZC).

The electro-reduction of  $\text{Co}^{2+}$  occurs at  $-0.68$  V from solution C, and at  $-1.04$  V for the Zn–Co alloys electrodeposition (solution ZC).

Fig. 2 shows the current density transients in potentiostatic regime (at  $-3.00$  V bias voltage) for the films deposited from solutions Z, C and ZC. We observe a continuous decrease in  $j$  on these curves, especially in the case of Co electrodeposition. This behavior suggests that the electrode is more or less passive by the deposition of a poorly conducting layer. Presumably, the film contains hydroxide precipitates, which are included in the deposited film at higher current densities, according to similar

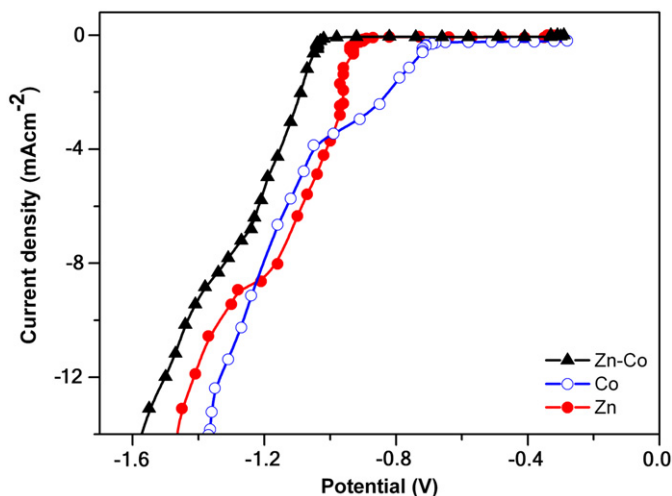


Fig. 1. Cathodic polarization curves from the sulfate bath of: ● zinc, ○ cobalt and ▲ Zn–Co alloy with a scan rate of  $3.3 \text{ mV s}^{-1}$ .

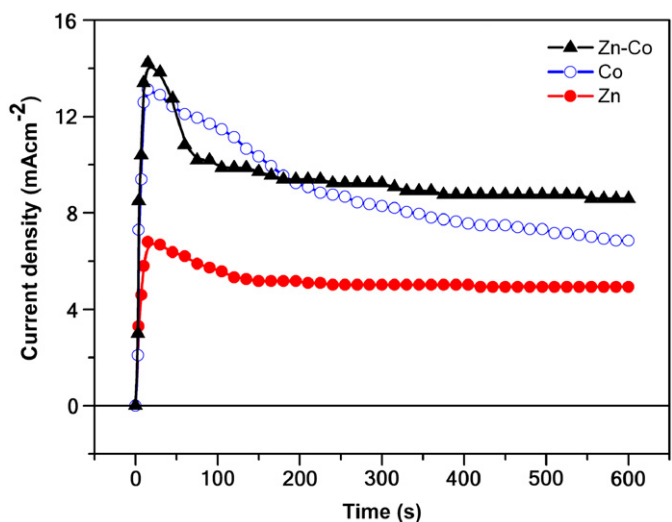


Fig. 2. Chrono-amperometric curves for the samples: ● zinc, ○ cobalt and ▲ Zn–Co alloy electrodeposited at 3.0 V bias voltages.

Table 1

Electrolyte composition ( $\text{g l}^{-1}$  in double distilled water) for Zn, Co and Zn–Co films electrodeposited, labeled Z, C and ZC, respectively.

Electrolytes	$\text{ZnSO}_4 \cdot 7\text{H}_2\text{O}$	$\text{CoSO}_4 \cdot 7\text{H}_2\text{O}$	$\text{Zn}(\text{O}_2\text{CCH}_3)_2(\text{H}_2\text{O})_2$	$\text{H}_3\text{BO}_3$	$\text{Na}_2\text{SO}_4 \cdot 10\text{H}_2\text{O}$	NaCl
Z	40	0	20	30	40	40
C	0	20	0	30	40	40
ZC	40	20	20	30	40	40

experiments [7]. This process is accompanied by a decay of the slope of the  $j(t)$  curves and the growth becomes more or less linear, with a mean value of slope depending on the applied voltage.

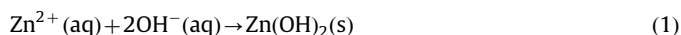
In the research for the present work we deposited the series of samples labeled for brevity S1–S7, as it is shown in Table 2, using the solutions and bias voltages shown in Table 1.

The effect of electrodeposition potential on the structure of the deposited films is shown in Figs. 3 and 4. In Fig. 3, we present as example the X-ray diffraction patterns of the Zn and Co films: S1 (a) and S3 (c). A comparison between the XRD patterns for the Zn samples S1 and S2 (between  $35.0^\circ$  and  $38.0^\circ$ ) is shown in Fig. 3(b), and for the Co samples S3 and S4 (between  $40.0^\circ$  and  $52.0^\circ$ ) are illustrated in Fig. 3(d). These XRD patterns indicate that the Zn and Co films are mainly of a hexagonal close packed (*hcp*) structure.

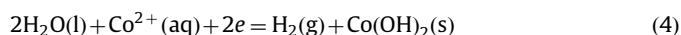
In Fig. 4, we present the X-ray diffraction patterns of the samples S5 (a) and S7 (b), from Zn–Co alloys deposited at 3.50 and 4.50 V bias voltages, respectively. In Fig. 4(c), a comparison between the patterns of the samples S5 and S7 (for  $35\text{--}38^\circ$ ) is shown. Depending on the electrodeposition parameters (especially on the bias voltage), the phases of the electrodeposited Zn–Co alloy is very complicated, and many phases coexist over a wide

range of compositions. The patterns in Figs. 3 and 4 indicate lines corresponding to *hcp* for zinc, zinc oxide (ZnO), zinc hydroxide ( $\text{Zn}(\text{OH})_2 \cdot 0.5\text{H}_2\text{O}$ ) and *hcp* for cobalt, cobalt hydroxide ( $\text{Co}(\text{OH})_2$ ), as it is marked by the Miller indices on the figures. On increasing the bias voltage of electrodeposition, the phase heterogeneity is increased, especially by inclusion in the deposit of Zn and Co hydroxides and Zn oxide (see for example Figs. 3(b,d) and 4(c)).

The formation of the hydroxides on the surface of Zn and Zn–Co electrodeposits can be explained by a sequence of reactions occurring during the film preparation. This process begins with the dissolution of Zn (anodic reaction) and the reduction of the oxygen dissolved in the solution. Zinc hydroxide is then formed by the reaction of  $\text{Zn}^{2+}(\text{aq})$  with  $\text{OH}^-(\text{aq})$ , according to the reaction (1). Because the solubility product of  $\text{Zn}(\text{OH})_2$  is very low, this compound precipitates on the surface and then it is possible to transform into zinc oxide [13]:



During Co electrodeposition in aqueous solutions onto the electrode, the formation of two types of solid products is possible as a result of the following reactions:



The relative contribution of reaction (4) to the current total depends on the pH of the solution and the presence of buffer additives [14].

From the diffraction patterns (Figs. 3 and 4), *a* and *c* cell parameters of the hexagonal structures were calculated. We have found the following values for cell parameters:  $a=2.66 \text{ \AA}$  and  $c=4.92 \text{ \AA}$  for  $\text{Zn}_{\text{hcp}}$  film,  $a=2.16 \text{ \AA}$  and  $c=4.08 \text{ \AA}$  for  $\text{Co}_{\text{hcp}}$  film and

**Table 2**

Notations for the series of samples deposited at different bias voltages from the solutions Z, C and ZC.

Samples	U bias (V)	Solution
S1	1.5	Z
S2	3	Z
S3	3	C
S4	4.5	C
S5	3.5	ZC
S6	4	ZC
S7	4.5	ZC

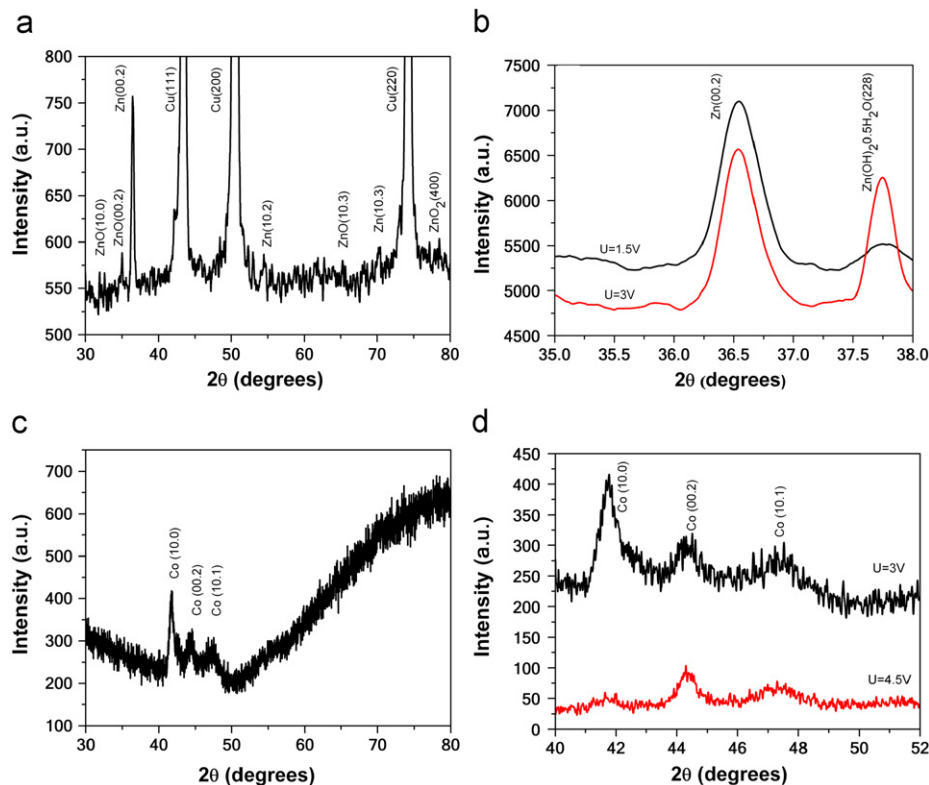


**Fig. 3.** X-ray diffraction patterns of the Zn and Co films: S1 (a) and S3 (c). A comparison between XRD patterns are presented in figures: (b) – for S1 and S2 (between  $35.0^\circ$  and  $38.0^\circ$ ) and (d) for S3 and S4 (between  $40.0^\circ$  and  $52.0^\circ$ ).

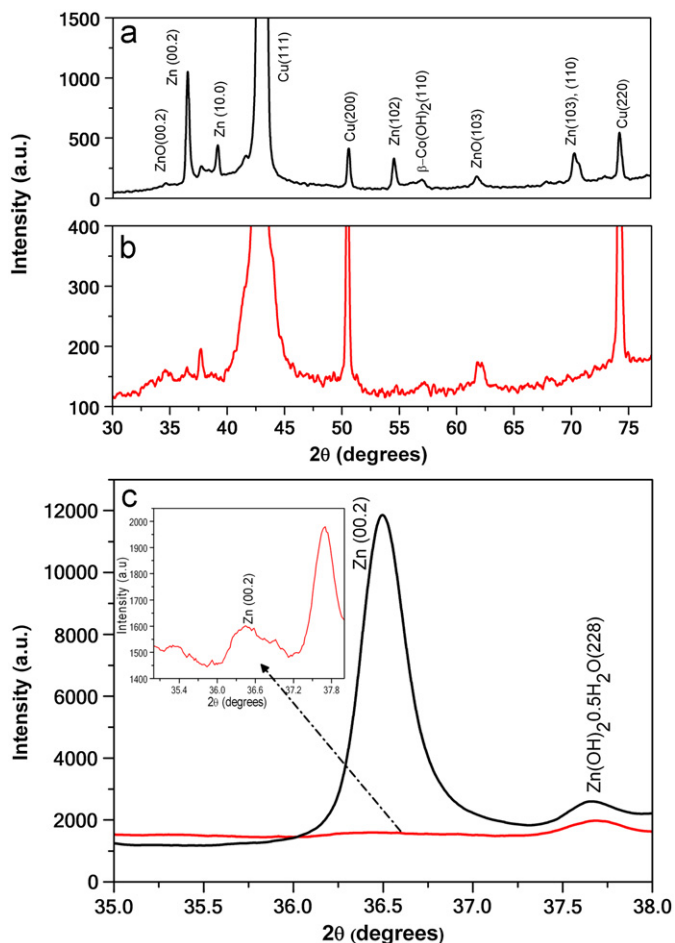


**Fig. 4.** X-ray diffraction patterns of the samples S5 (a) and S7 (b), from Zn–Co alloys granular films deposited at 3.50 and 4.50 V, respectively. (c) shows the comparison between the patterns of the two samples for 35–38°.

$a=2.75 \text{ \AA}$  and  $c=4.92 \text{ \AA}$  for Zn–Co film (S5, S7), which show a much distorted structure. XRD showed, together with the lines of the substrate, the lines of an undistorted hexagonal zinc  $\eta$ -phase, as it was found in Ref. [15] and  $\text{Co}_{hcp}$  phase, which confirmed our hypothesis concerning formation of Zn and Co granular films. The cell parameter modification affected mainly the  $c$  crystallographic axis, which was clearly lower than that of pure zinc.

The particle sizes of the films were calculated using the Scherer equation (5) [7,12]:

$$D = \frac{0.9\lambda}{\beta \cos\theta} \quad (5)$$

where  $\lambda$ ,  $\theta$  and  $\beta$  are the X-ray wavelength (1.5406 Å), diffraction angle and full width at half the maximum (FWHM) of the Zn, Co and Zn–Co alloy peaks, respectively. The average grain size of the crystallites from the zinc deposit was 25 nm, for the cobalt deposit was 16 nm and it was 27 nm for the zinc–cobalt alloy granular thin films.

Atomic force microscopy (AFM) has also been used to investigate the surface morphology of Zn, Co and Zn–Co alloy films. Some AFM phase images of the Zn, Co and Zn–Co electrodeposited samples (S2, S3 and S7) are shown in Fig. 5 (topography-left (a,c,e) and phase images-right (b,d,f)).

It is known that a phase image, collected simultaneously with a topographical image, shows maps the local changes in the material's physical or mechanical properties of the material. In the left image, we see the many interesting surface features of the film. When combined with the phase image (right), we can tell

which features are of similar chemical composition. This allows determining whether the surface features may be the result of a specific chemical component, or if the surface is homogeneous. The phase signal changes when the probe encounters regions of different composition.

It is obvious that the roughness ( $R_{ms}$ ) of the zinc is smaller, ( $R_{ms}=15.4 \text{ nm}$ ), than that of the cobalt film, ( $R_{ms}=20.1 \text{ nm}$ ) and of the zinc–cobalt alloy,  $R_{ms}=23.5 \text{ nm}$  under the same conditions. Also, in the case of Zn–Co alloy, crystalline grains formed at film surface are larger in size. Phase images obtained for the samples of Zn, Co (represented in Fig. 5b,d) demonstrate a relatively homogeneous disposition of phases on the surface of the layer. The image from Fig. 5f suggests the deposition of different phases starting from different nucleation sites, because the contrast in the phase image is primarily a result of material inhomogeneity. This separation of phases was predicted since the examination of Zn–Co alloy phase diagram. We conclude that the granular Co–Zn films may consist of Co micro- or nanoparticles embedded in a heterogeneous zinc, zinc oxide and hydroxide matrices, and have varied particle sizes, and crystalline orientations. The heterogeneity of films could be a favorable condition to increase the film magnetoresistance.

From the preliminary SEM experiments, the film composition depended on electrodeposition potential. For example, the films deposited at 3.5 V contain 92 at% Zn, 8 at% Co and those deposited at 4.5 V contain 84 at% Zn, 16 at% Co.

The chemical composition of electrodeposited Zn–Co alloys and the chemical state of constituent elements were investigated using the X-ray photoelectron spectroscopy (XPS). A typical XPS spectrum of electrodeposited Zn–Co alloys is shown in Fig. 6(a). It reveals the presence of zinc ( $\text{Zn } 2p_{3/2}$  and  $\text{Zn } 2p_{1/2}$  peaks), cobalt ( $\text{Co } 2p_{3/2}$  and  $\text{Co } 2p_{1/2}$  peaks) and oxygen incorporated in the Zn–Co matrix ( $\text{O } 1s$  peak).

In the high-resolution spectra of Zn 2p (Fig. 6(b)) both the Zn  $2p_{1/2}$  and the Zn  $2p_{3/2}$  covers can be deconvoluted into two distinctive components corresponding to zinc oxide (1021.9 eV for Zn  $2p_{3/2}$  and 1044.6 eV for Zn  $2p_{1/2}$ ) and hydroxide, (1023.2 eV for Zn  $2p_{3/2}$  and 1046.2 eV for Zn  $2p_{1/2}$ ), respectively.

As it is seen in Fig. 6(c), the peak O 1s is asymmetric, which reveals the presence of a multi-component peak of oxygen and it can be decomposed into three component peaks. The right centered at 530.7 eV (O1) can be associated with the zinc oxide groups, the medium centered at 531.7 eV (O2) is related to the presence of hydroxyl type groups, and the left centered at 532.9 eV (O3) could be assigned to the presence of loosely bound oxygen on the surface of Zn–Co films, as it was established in Ref. [16].

The Co  $2p_{3/2}$  and Co  $2p_{1/2}$  peaks are localized at the binding energies of 778.1 and 792.2 eV, respectively (Fig. 6(d)), each of them being determined by three Co-containing components obtained after deconvolution. Metallic Co is localized at 778.1 eV for Co  $2p_{3/2}$  and 792.5 eV for Co  $2p_{1/2}$ ; the energy difference between peaks is around 15.05 eV, and it proved that Co exists as a metal cluster in our electrodeposited Zn–Co alloys [17]. The  $\text{Co(OH)}_2$  groups were localized at 782.1 and 797.8 eV and the two satellites also appeared at about 786.9 and 803.4 eV.

The magnetic measurements were carried out at room temperature with a torsion magnetometer in 300 kA/m maximum field. Fig. 7 shows as an example the torsion magnetometer curves of the samples S6 and S7 for Zn–Co alloys granular films. Fig. 7(a) and (b) shows the static torque curves performed for clockwise and anticlockwise rotation of the magnetic field, for the samples (S6 see Fig. 7(a) and S7 (Fig. 7(b)). The shape of the curves obtained by the torsion magnetometer was a very sensitive function of the sample magnetic microstructure. The film

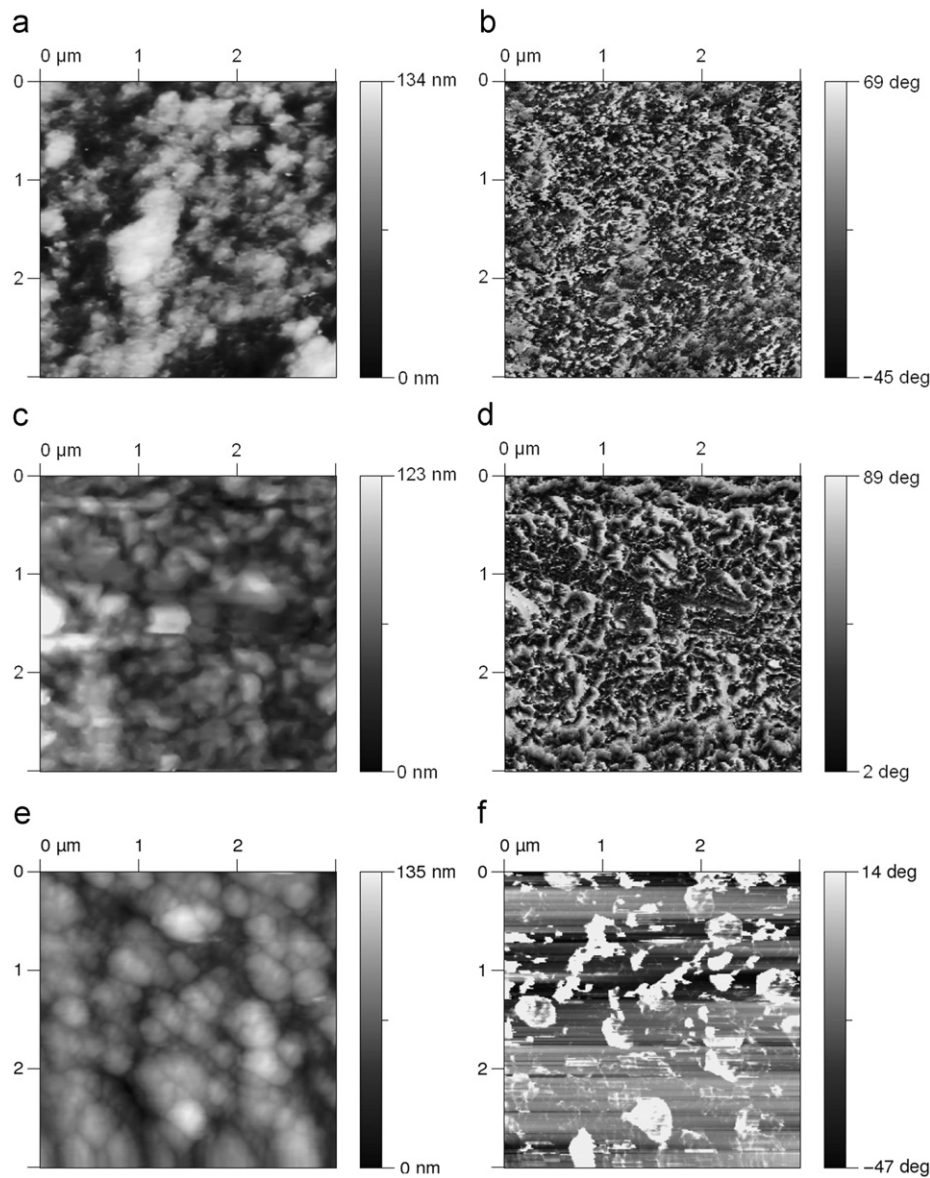


**Fig. 5.** The AFM images of Zn (a,b), Co (c,d) and Zn–Co (e,f) films electrodeposited on copper substrate (topography-left (a,c,e) and phase images-right (b,d,f)).

plane was placed perpendicular on the field-rotation plane; e.g. the torque was around an arbitrary axis, which was parallel to the film plane. From the shape of torsion curves we deduced the existence of uniaxial anisotropy and antiferromagnetic type interactions (evidenced by the  $\sin \theta$  shape of the torque curves in low magnetic fields and the increase in the rotational hysteresis losses in high magnetic fields). The samples display an out of plane magnetic anisotropy evidenced by torque magnetometry. The shape of the torsion curves (with very high rotational hysteresis losses in high magnetic fields) proves the presence of the antiferromagnetic type interaction between the crystalline grains.

The hysteresis loops and magnetic susceptibility measurements of Zn–Co alloy films were performed using an ac induction type device with computerized data acquisition system (50 Hz, maximum field applied in the plane of the samples 60 kA/m). Fig. 8(a),(b) shows the curve of magnetization ( $M$ ) versus field ( $H$ ) at room temperature for Zn–Co thin films and the comparison between the susceptibility curves functions by magnetic field, respectively, for the same samples. Fig. 8(a) shows the hysteresis loops for the Zn–Co alloy films (samples S6 and S7) at different

voltages. The shapes of  $M(H)$  loops and of the susceptibility curves  $\chi(H)$  modify, this being a function of the microstructure of the sample, changed according to the applied voltage control. The small changes in the shape of  $(dM/dt)$  versus  $H$  reflect changes in the magnetization processes and in the switching properties of the films.

To explain this behavior, it is necessary to take into account the main physical properties of the grains and of the exchange interactions between grains. Thin granular films of Zn–Co alloys can contain two ferromagnetic phases (Co and Co–Zn solid solution). This constitution possibly arises because different nucleation sites determined by different local conditions on the cathode/solution interface may produce grains with various compositions and structures separated by inhomogeneous frontiers containing Co and Zn hydroxides. The anomalous deposition in Zn–Co system occurs due to the formation and adsorption of hydroxide species on the cathode inhibits cobalt electrodeposition, favoring that of zinc; this could explain the local inhomogeneity of the cathode surface. On the other hand, the presence of Co into Zn plating baths modifies the morphology of the deposits because of their influence on the growth of the initial crystal nuclei.

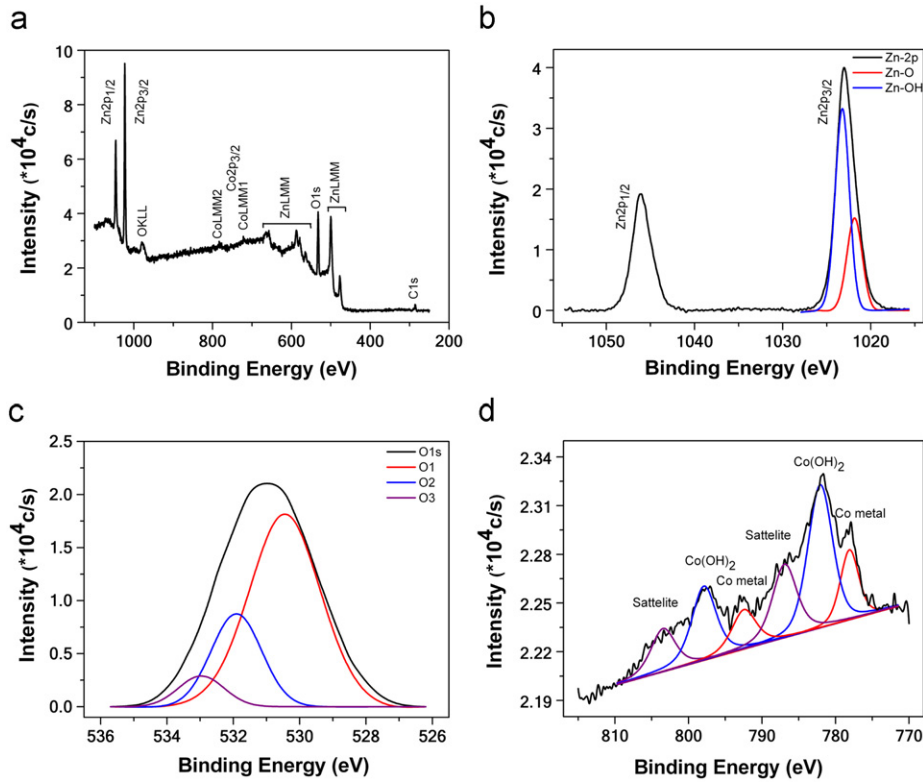


**Fig. 6.** X-ray photoelectron spectra for Zn–Co alloy film (S7). (a) Represents the general X-ray photoelectron spectra; whereas (b), (c) and (d) represent the deconvoluted core level spectra of Zn (2p), O (1s) and Co (2p), respectively.

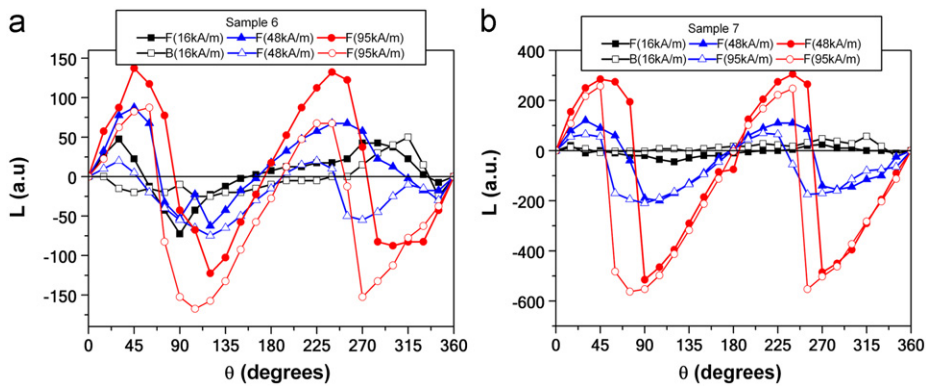


**Fig. 7.** Torque curves for the samples S6 (a) and S7 (b) plotted for clockwise rotation from 0° to 360° (F) and anticlockwise rotation from 360° to 0° (B). The torque curves were measured for the fields: 16, 48 and 95 kA/m (marked in the legend).

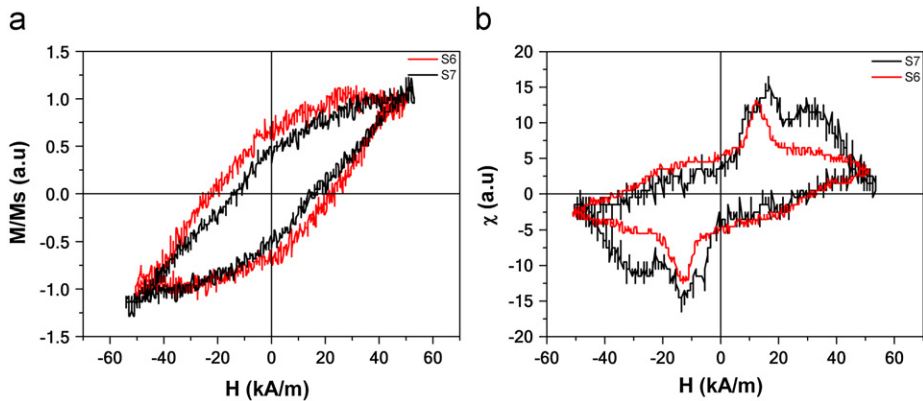


**Fig. 8.** Comparison between hysteresis curves of the samples S6 and S7 (from Zn–Co alloy) deposited at 4.0 and 4.5 V, respectively, (a) and (b) show comparison between the susceptibility curves as a function of magnetic field, for the samples S6 and S7.

#### 4. Conclusions

The homogeneous Zn–Co alloys were electrodeposited on Cu substrate and we have found that the composition of deposits was controlled mainly by the applied voltage control. Taking into account the values of the applied voltage, two samples obtained at 3.5 V (S5) of Zn–Co alloy and 4.5 V (S7), respectively, were presented as an example in this work. In the same preparation conditions we have obtained granular films with different compositions, only by the variation of the applied voltage. The average size of the zinc, cobalt and Zn–Co alloys electrodeposited particles were obtained by X-ray diffraction analysis. Detailed XPS analysis indicated the presence of zinc oxide (ZnO) in the samples of Zn and Zn–Co alloys. The shape of the torsion curves proved the presence of an antiferromagnetic type interaction between the crystalline grains. The microstructure and magnetic properties of the Zn–Co alloys depend strongly on the nature of the deposited sample on different applied voltage.

#### References

- [1] A.R. de Moraes, D.H. Mosca, N. Mattoso, W.H. Schreiner, A.J.A. de Oliveira, W.A. Ortiz, *Physica B: Condensed Matter* 320 (2002) 199.
- [2] S. Kenane, J. Voiron, N. Benbrahin, E. Chainet, F. Robaut, *Journal of Magnetism and Magnetic Materials* 297 (2006) 99.
- [3] H.B. Muralidhara, Y.Arthoba Naik, *Bulletin of Materials Science* 31 (2008) 585.
- [4] E. Gomez, E. Valles, *Journal of Electroanalytical Chemistry* 421 (1997) 157.
- [5] W. Tian, F.Q. Xie, X.Q. Wua, Z.Z. Yangb, *Surface and Interface Analysis* 41 (2009) 251.
- [6] Pedro de Lima Neto, Adriana N. Correia, Regilany P. Colares, Walney S. Araujo, *Journal of the Brazilian Chemical Society* 18 (6) (2007) 1164.
- [7] J.B. Bajat, S. Stankovic, B.M. Jokic, *Journal of Solid State Electrochemistry* 13 (2009) 755.
- [8] A. Brenner, *Electrodeposition of Alloys*, vol. 2, Academic Press, New York, 1963, pp. 194.
- [9] J.B. Bajat, S. Stankovic, B.M. Jokic, S.I. Stevanovic, *Surface and Coatings Technology* 204 (2010) 2745.
- [10] A. Cunha, S.D. Carpenter, J.Z. Ferreira, D.E.O.S. Carpenter, J.P.G. Farr, *Corrosion Engineering, Science and Technology* 38 (2003) 313.
- [11] Fenglan Song, Lianrong Huang, Donghua Chen, Wanjun Tang, *Materials Letters* 62 (2008) 543.
- [12] O. Lupan, L. Chow, S. Shishiyanu, E. Monaico, T. Shishiyanu, V. Şontea, B.Roldan Cuenya, A. Naitabdi, S. Park, A. Schulte, *Materials Research Bulletin* 44 (2009) 66.
- [13] Pedro De Lima-Neto, Adriana N. Correia, Regilany P. Colares, Walney S. Araujo, *Journal of the Brazilian Chemical Society* 18 (2007) 1164.
- [14] M. Lafouresse, A. Medvedev, K. Kutuso, W. Schwarzacher, A. Masliy, *Russian Journal of Electrochemistry* 43 (7) (2007) 856.
- [15] E. Gomez, X. Alcobe, E. Valles, *Journal of Electroanalytical Chemistry* 505 (2001) 54.
- [16] Lisha Zhang, Zhigang Chen, Yiwen Tang, Zhijie Jia, *Thin Solid Films* 492 (2005) 24.
- [17] A. El Manouni, M. Tortosa, F.J. Manjon, M. Mollar, B. Mari, J.F. Sanchez-Royo, *Microelectronics Journal* 40 (2009) 268.